Available online at www.sciencedirect.com
SCIENCE DIRECT®

Journal of the European Ceramic Society 24 (2004) 1919–1923
www.elsevier.com/locate/jeurceramsoc

Partial electronic and ionic conduction in nanocrystalline ceria: role of space charge

Sangtae Kim*, Joachim Maier

Max-Planck-Institut für Festkörperforschung, Heisenbergstr. 1, 70569 Stuttgart, Germany

Abstract

The total electrical conductivities of Gd-doped (0.15 mol%) and nominally pure nanocrystalline CeO_{2-x} ceramics (~30 nm grain size) were measured by impedance spectroscopy as a function of temperature and oxygen partial pressure. Careful separation of the partial ionic and electronic contributions using an electronically blocking cell allowed for a clear distinction between potential explanations. It is shown that unlike competing models the space charge model explains all the experimental features not only qualitatively but also quantitatively.

Keywords: CeO_2; Electrical conductivity; Interfaces

1. Introduction

Of particular interest regarding nano-structured electroceramics is the fact that their conduction properties may become interfacially controlled due to a high density of interfaces (grain boundaries), and that the distance between interfaces is expected to become a further control parameter determining the occurrence of size effects on the overall conductivity.[1–3]

Considering its technological relevance, it is not surprising that CeO_{2-x} is one of the most intensively studied oxides in nanocrystalline state.[4–7] According to the literature, experimental results agree in the conclusion that the overall conductivity (with lower activation energy), attributed to the electrons, e', is significantly increased compared to that of a single crystal or a microcrystalline ceramic. Discrepancies, however, are met as far as the conduction mechanism is concerned.

The simplest realistic approach is the abrupt core space charge model[8] in which the structure is assumed to change as a step function: Not only are core structure and hence defect chemistry and mobilities therein different from the bulk, but also does the "contact" of two structurally different regions imply a charge redistribution. The excess charge in the core will be compensated by a diffuse charge distribution in the space charge zones (scz).

Only if the charging can be neglected the grain boundary core (gc) can be treated as a neutral layer with own intrinsic defect concentrations and mobilities. This *neutral layer model* has been applied to explain the above conductivity effects. Indeed intuition and calculation[9] support assumption of decreased formation enthalpies for oxygen vacancy, $V_O^{\bullet\bullet}$, and e'. An increased carrier concentration and assuming similar mobilities as in the bulk the increased n-type conductivity could be qualitatively explained.[4]

On the other hand, space charge potentials, $\Delta\phi(0)$, observed for microcrystalline CeO_{2-x}[10] being of the order of ~0.3 V necessitate a sever charging. The situation can be treated in a straightforward way if one now conversely assumes that scz (and not the core charge carriers) dominate the conductivity effects (in the following called *the space charge model*). This is a reasonable assumption since the mobilities in bulk CeO_{2-x} are high and expected to be lowered by softening short and long range order. In fact positive $\Delta\phi(0)$ directly predict an increased *n*-type conductivity as discussed by Tschoepe.[7]

It is apparent now that an answer as to which model is more plausible requires a direct separate determination of partial conductivities and quantitative analyses of their behavior based on the models. Especially the different situation of the ionic carrier is striking: While in the neutral layer model the ionic as well as the electronic conductivity should be enhanced (given

* Corresponding author. Tel.: +49-711-689-1764; fax: +49-711-689-1722.
E-mail address: s.kim@fkf.mpg.de (S. Kim).

0955-2219/$ - see front matter © 2003 Elsevier Ltd. All rights reserved.
doi:10.1016/S0955-2219(03)00525-9

similar mobilities as in the bulk)[12] in gc (Fig. 1 a), a severe depression of the ionic conductivity (due to depletion of $V_O^{\bullet\bullet}$) should occur in scz (Fig. 1b). It will be shown that the results can be consistently explained by the space charge model in all details (unlike the neutral layer model). A more detailed report will be given.[13]

2. Experimental

Gd-doped (0.15 mol%, *n*-CGO) and nominally pure nanocrystalline CeO_{2-x} (*n*-CeO_2) powder was precipitated by decomposing $Ce(N0_3)_3{\cdot}6H_2O$ (Aldrich, 99.99%) and $Gd(NO_3)_3{\cdot}6H_2O$ (Aldrich, 99.99%) (See Ref. 15 for detail). The particle size of the synthesized powder (determined independently by Fourier analysis of XRD peak profiles, Brunauer–Emmett–Teller (BET) N_2 absorption method, and transmission electron microscopy (TEM)) was about 8 nm. The measured density of the disk-shaped samples (average grain size of ~30 nm based on XRD Fourier analysis) of both *n*-CGO and *n*-CeO_2, prepared by cold isostatic pressing (CIP, 800 Mpa) followed by pressureless sintering (800 °C for 30 mm), was about 90% of the theoretical value.

The total electrical resistance of the samples was measured using a Solatron 1260 impedance analyzer as a function of P_{O_2} and T. The partial ionic resistance of the samples was measured by potentiostatically polarizing the electronically blocking cell, *Pt*/*n*-CeO_2 (or *n*-CGO)/YSZ/Pt (for preparations in detail, see Ref. 13). Owing to the high aspect ratio of the ceria samples of ~15 (based on ~7 mm in diameter and 0.5–0.7 mm in thickness) a sealing was not essential. During polarizing the cell, a Keithley 230 voltage source was used, and the electrical currents were measured by a Keithley 617 electrometer.

3. Results and discussion

3.1. Electrical properties of n-CGO

A typical impedance spectrum of nominally Gd-doped CeO_{2-x} (*n*-CGO) shown in Fig. 2 was found to consist of a small high frequency arc together with a large low frequency one. The parameters resulting from fitting those arcs are summarized in Table 1. Both electrical resistances, R_1 and R_2, were independent of P_{O_2} (Fig. 3a). However, the activation energy of R_2 was substantially higher compared to that of R_1 as indicated (in terms of the resistivity, ρ) in Fig. 3b. The partial ionic dc resistance, R_v^{dc} (*n*-CGO), of *n*-CGO measured from the cell, Pt/*n*-CGO/YSZ/Pt, corresponds for all P_{O_2}-values and temperatures to the sum of R_1 and R_2, hence being independent on P_{O_2} (electrode impedances of the cell are found to be negligibly small according to its impedance spectrum, which was identical to Fig. 2).

Of particular interest regarding Fig. 2 is the appearance of the low frequency arc, characteristic of blocking grain boundaries (the high frequency arc can be attributed to the bulk ionic response, see Ref. 13 for detail). As emphasized above, in the neutral layer model, such a low frequency arc would not be expected (see Fig. 1a for detail). On the other hand, in the space charge model, a strong resistance to the ionic conduction, dominated by

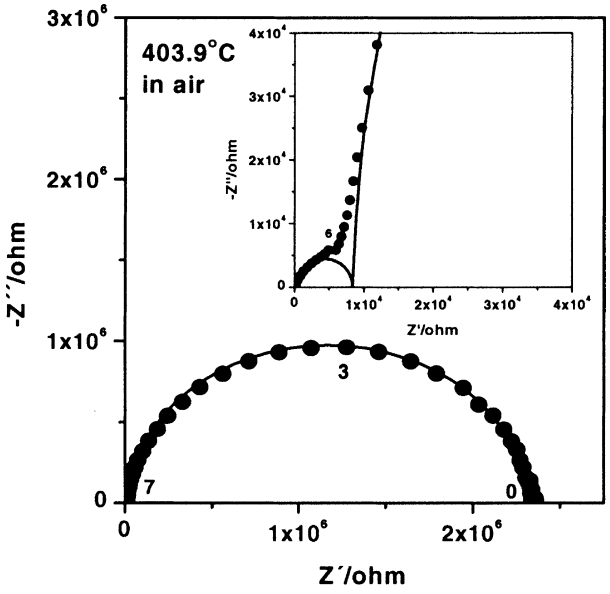

Fig. 2. A typical impedance spectrum of *n*-CGO. Indicated numbers give the logarithm of the measurement frequency (Hz).

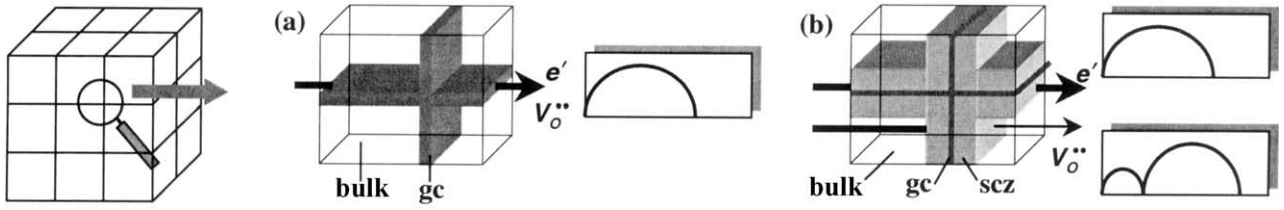

Fig. 1. (a) the neutral layer model: both electronic and ionic transport occur through the parallel gc with enhanced charge carrier (e' and $V_O^{\bullet\bullet}$) number (similar mobilities in gc were assumed). (b) the space charge model: while the electronic conduction should be determined by parallel space charge zones (the mobility of the core charge is neglected), the ionic conduction should almost exclusively proceed along the bulk path as the space charge zones are strongly depleted of $V_O^{\bullet\bullet}$. Note, however, that for a long-range conduction of $V_O^{\bullet\bullet}$, extreme boundary resistances (due to the serial depletion zones) have to be overcome and thus will show up in the impedance spectrum as a separate low frequency arc.

the serial scz, should appear in the impedance spectrum as a separate arc (see Fig. 1b for detail). Owing to $R_1 + R_2 \approx R_v^{dc}$ (*n*-CGO), the low frequency arc must reflect a ionic grain boundary resistance (chemical capacitances are neglected),[13] and therefore it is exactly what we expect from the space charge considerations. In addition, since other possible causes (e.g. an insulating amorphous Si-layer and/or pores in gc, the activation energy (Fig. 3b) show that it is not current constriction!) were found to be irresponsible[13] for the low frequency arc shown in Fig. 2, we focus, in the following, on the space charge model and show that it quantitatively accounts all the effects observed.

Concentration profiles in scz are in general described by Gouy–Chapman or Mott–Schottky models.[11] Since the expected concentration profiles in *n*-CGO are in agreement with the latter,[13] $\Delta\phi(0)$ can be computed from the ratio of grain boundary resistivity, ρ_{gb}, to the bulk resistivity, ρ_∞, given as;[14]

$$\frac{\rho_{gb}}{\rho_\infty} = \frac{\exp(ze\Delta\phi(0)/k_BT)}{2ze\Delta\phi(0)/k_BT} \quad (1)$$

being about 0.3 V for *n*-CGO at 404 °C, which is consistent with the value observed for microcrystalline CeO_2 (~0.3 V).[10]

3.2. Electrical properties of n-CeO_2

As the number of e' in scz is much higher for *n*-CeO_2 (nominally pure) than for *n*-CGO, the boundary path is expected to bypass the bulk path, causing the low frequency arc to be absent. This is now exactly what is observed in Fig. 4 (there is only one arc), and Fig. 5a: the measured overall conductivity, σ_m, is at least partly electronic (negative P_{O_2} dependence), and is higher than the partial ionic value, $\sigma_{v\infty}$, (showing a zero P_{O_2} dependence, *i.e.* extrinsic) obtained from the blocking cell, Pt/*n*-CeO_2/YSZ/Pt (the lower index m always refers to the total sample average. Subscripts v (or n) refers to $V_O^{\bullet\bullet}$ (or e'), and ∞ denote the bulk). By subtracting $\sigma_{v\infty}$[13] from σ_m (as shown in Fig. 5) we obtain a direct (proportional) measure of $\sigma^{||}_{m,n}$ whose value (at 490 °C in air) was increased by about a factor of 3 compared to the corresponding value of an undoped single crystal ceria[15] (Superscript || (or ⊥) denotes parallel (or series) to the interface). Note that $\sigma^{||}_{m,n}$ is at least a factor of 10 smaller than the conductivity in scz (the fact we do not see depletion effects in the ionic conductivity (see Fig. 5a at higher P_{O_2}) was attributed to grain boundary wetting).[13]

Table 1
The resulting parameters from a fit of measured impedance spectra

Sample	R_1 (Ω)	C_1 (F)	R_2 (Ω)	C_2 (F)
n-CGO[a]	7.9×10^3	1.1×10^{-11}	2.2×10^6	5.8×10^{-11}
n-CeO_2[b]	7.3×10^5	1.2×10^{-11}		

[a] 404 °C.
[b] 432 °C.

3.3. Quantitative analyses of P_{O_2} and T- dependencies of the space charge effect

In the Mott-Schottky model, the effective electronic conductivity and the ionic resistivity are given as[16] $\sigma^{||}_{m,n} \propto c_{n0}/[2\ln(c_{n0}/c_{n\infty})]$ and $\rho^{\perp}_{m,v} \propto 1/[2c_{v0}\ln(c_{v0}/c_{v\infty})]$, respectively (0 refers to the first layer of the bulk from *gc*). Owing to the relation $c_0 = c_\infty \exp(-ze\Delta\phi(0)/k_BT)$,[11] in case of *n*-CGO, $\rho^{\perp}_{m,v}$ is expected (from Eq. (6), see below, with $2[V_O^{\bullet\bullet}] = [Gd']$) to depend on P_{O_2} according to

$$\partial\ln\rho^{\perp}_{m,v}/\partial\ln P_{O_2} \cong -\partial\ln c_{v\infty}/\partial\ln P_{O_2} = 0 \quad (2)$$

(since $\partial\Delta\phi(0)/\partial P_{O_2} \approx 0$[13]), as indeed seen in Fig. 3a.

Similarly, the temperature dependence of $\rho^{\perp}_{m,v}$ yields

$$k_B\partial\rho^{\perp}_{m,v}/\partial T^{-1} = E^{\perp}_{m,v} = E_{v\infty} + 2e\left[\Delta\phi(0) + T^{-1}\partial\Delta\phi(0)/\partial T^{-1}\right] \quad (3)$$

and thus the T-dependence of the barrier height follows as $T^{-1}\partial\Delta\phi(0)/\partial T^{-1} \approx 0.1$ V ($\Delta\phi(0) \approx 0.3$ V, see also

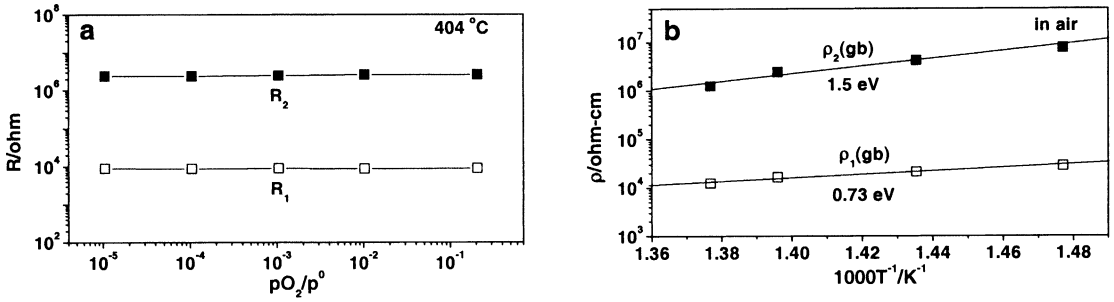

Fig. 3. (a) P_{O_2} dependence of the resistances obtained from the fits of impedance spectra of *n*-CGO; (b) the temperature dependence of its resistivities.

Fig. 3b).

On the other hand, $\sigma^{\perp}_{m,v}$ of n-CeO_2 reveals a P_{O_2} dependence which is almost exactly $-1/4$ (Fig. 5a). Assuming $\Delta\phi(0)$ to be similar as in the case of n-CGO, we indeed expect (from Eq. (6), see below, in still extrinsic regime) the following:

$$\partial \ln \sigma^{\parallel}_{m,n}/\partial \ln P_{O_2} \cong \partial \ln c_{n\infty}/\partial \ln P_{O_2} = -0.25 \quad (4)$$

Finally, according to $E_{n\infty} = 2.37$ eV,[15] the temperature dependence of $\sigma^{\parallel}_{m,n}$ reads

$$k_B \partial \ln \sigma^{\perp}_{m,n}/\partial T^{-1} \cong E_{n\infty} + e\left(\Delta\phi(0) + T^{-1}\partial\Delta\phi(0)/\partial T^{-1}\right) \approx -2.0 \text{ eV} \quad (5)$$

which is almost exactly the experimental value of -1.9 eV (Fig. 5b). Note the excellent agreement between the values predicted by the model and those observed experimentally for all cases.

3.4. Consistency check

Owing to the fact that after all we refer to the same electrical potential profiles and the same local conditions, c_{n0} or c_{v0}, are (in local equilibrium) subjected to the following consistency condition

$$c^2_{n0}c_{v0} = c^2_{n\infty}c_{v\infty} = K(T)P^{-1/2}_{O_2} \quad (6)$$

where $K(T)$ is the bulk equilibrium constant for the defect formation reaction,

$$O^x_O \leftrightarrow V^{\bullet\bullet}_O + 2e' + 1/2O_2. \quad (7)$$

As far as the P_{O_2} and T-dependences are concerned, it is required that[15]

$$2\left(\partial \ln \sigma^{\parallel}_{m,n}/\partial P_{O_2}\right) + \left(\partial \ln \sigma^{\perp}_{m,v}/\partial P_{O_2}\right) = -1/2 \quad (8)$$

$$k_B\left[2\left(\partial \ln \sigma^{\perp}_{m,n}/\partial T^{-1}\right)\right] + \left(\partial \ln \sigma^{\perp}_{m,v}/\partial T^{-1}\right) = \Delta H^0_{f,v} + 2h_n + h_v \quad (9)$$

where h is the migration energy. Since $\partial \ln \sigma^{\parallel}_{m,n}/\partial P_{O_2} = -1/4$ and $\partial \ln \sigma^{\perp}_{m,v}/\partial P_{O_2} = 0$, Eq. (8) is indeed satisfied. According to literature values for h_n, ($\sim$0.4 eV)[17] an h_v ($\sim$0.6 eV),[18] we estimate from Eq. (9) a ΔH^0_{fv} value of $\sim$3.9 eV as l.h.s. of Eq. (2) is $\sim$5.3 eV. And such estimated value is indeed very close to the experimental value of 3.94 eV measured for a polycrystalline CeO_{2-x}.[15]

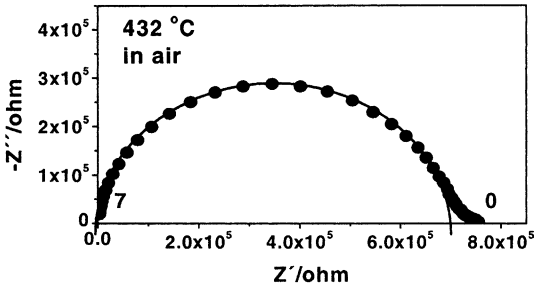

Fig. 4. A typical impedance spectrum of n-CeO_2. Indicated numbers give the logarithm of the measurement frequency (Hz).

4. Conclusions

It is shown that in contrast to the neutral layer model the space charge model explains all the experimental features in detail. Assuming a Mott–Schottky model we successfully explain the impedance responses of doped and nominally pure nanocrystalline CeO_{2-x}. The oxygen partial pressure and temperature dependencies of bulk and boundary conductivities can be quantitatively anylyzed. In addition, the consistency criteria that connect the boundary values of ionic (depletion) and

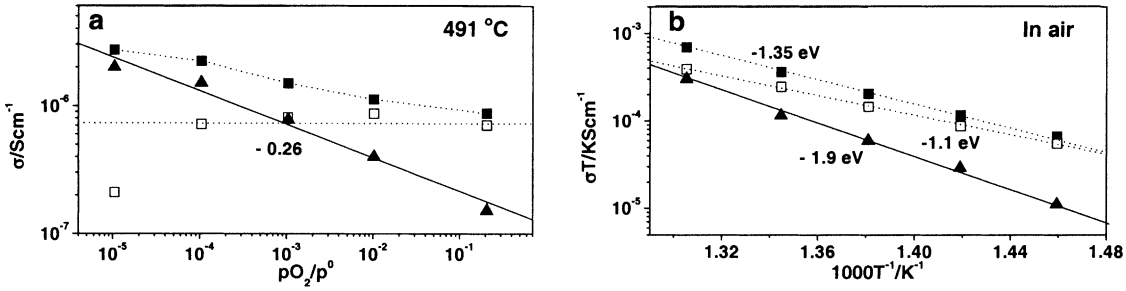

Fig. 5. (a) The oxygen partial pressure and (b) the temperature dependence of the effective partial ionic and electronic conductivities, and the total conductivity: σ_m(■), $\sigma_{v\infty}$(□) and $\sigma^{\parallel}_{m,n}(=\sigma_m - \sigma_{v\infty})$(▲).

electronic (accumulation) profiles, being independently measured, are excellently fulfilled.

References

1. Maier, J., Point defect thermodynamics: macro- vs. nanocrystals. *Electrochemistry*, 2000, **68**, 395–402.
2. Maier, J., Nano-sized mixed conductors (aspects of nano-ionics. Part III). *Solid State Ionics*, 2002, **148**, 367–374.
3. Tuller, H. L., Ion conduction in nanocrystalline materials. *Solid State Ionics*, 2000, **131**, 143–157.
4. Chiang, Y.-M., Lavik, E. B., Kosacki, I., Tuller, H. L. and Ying, J. Y., Defect and transport properties of nanocrystailine CeO_{2-x}. *Applied Phys. Lert.*, 1996, **69**(2), 185–187.
5. Hwang, J.-H. and Mason, T. O., Defect chemistry and transport properties of nanocrystalline cerium oxide. *Z. Phys. Chem.*, 1998, **207**, 21–38.
6. Kosacki, I., Suzuki, T., Petrovski, V. and Anderson, H., Electrical conductivity of nanocrystalline ceria and zirconia thin films. *Solid State Ionics*, 2000, **136–137**, 1225–1233.
7. Tschöpe, A., Grain-size dependent conductivity of polycrystalline cerium oxide. II. Space charge model, *Solid State Ionics*, 267–280.
8. Jamnik, J., Maier, J. and Pejovnik, S., Interfaces in solid ionic conductors: equilibrium and small signal picture. *Solid State Ionics*, 1995, **75**, 51–58.
9. Sayle, T. X. T., Parker, S. C. and Catlow, C. R. A., The roleof oxygen vacancies on ceria surfaces in the oxydation of carbon monoxide. *Surf Sci.*, 1994, **316**, 329–336.
10. Guo, X., Sigle, W. and Maier, J., The blocking grain boundaries in yttria-doped and undoped ceria ceramics of high purity, submitted to *J. Am. Ceram. Soc.*
11. Maier, J., Ion conduction in space charge regions. *Prog. Solid State. Chem.*, 1995, **23**, 171–263.
12. Tschoepe, A., Grain-size dependent thermopower of polycrystalline cerium oxide. *Solid State Ionics*, 2002, **149**, 261–273.
13. Kim, S. and Maier, J., On the conductivity mechanism of nanocrystalline ceria. *J. Electrochem. Soc.*, 2002, **149**(10), J73–J83.
14. Guo, X. and Maier, J., Grain boundary blocking effect in zirconia: a Schottky barrier analysis. *J. Electrochem. Soc.*, 2001, **148**(3), E121–E216.
15. Tuller, H. L. and Nowick, A. S., Doped ceria as a solid state electrolyte. *J. Electrochem. Soc.*, 1975, **122**, 255–259.
16. Kim, S., Fleig, J. and Maier, J., Space charge conduction: Simple analytical solutions for ionic and mixed conductors and application to nanocrystalline ceria. *Phys. Chem. Chem. Phys.*, 2003, **5**, 2268–2273.
17. Tuller, H. L. and Nowick, A. S., Small polaron electron transport in reduced CeO_2 single crystal. *J. Phys. Chem. Solids*, 1977, **38**, 859–867.
18. Wang, D. Y., Park, D. S., Griffith, J. and Nowick, A. S., Oxygen conductivity and defect interactions in yttria-doped ceria. *Solid State Ionics*, 1981, **2**, 95–105.